UDC 550.8.05:622.831.3
DOI: 10.15587/2706-5448.2024.301709

Said Derbane,
Mouloud Mansouri,
Salah Messast

CONTRIBUTION TO MICROMECHANICAL MODELING OF THE SHEAR WAVE PROPAGATION IN A SAND DEPOSIT

The object of study is the vertical wave propagation in a sand deposit. This paper is aimed at analyzing the vertical wave propagation in a sand deposit through micromechanical modeling that inherently takes account of intergranular slips during deformation. Such a problem, which is part of the general framework of wave propagation in the soil, has long been analyzed using continuum models based on approximate behavior laws. For this purpose, a 2D Discrete Element Method (DEM) model is developed. The DEM model is based on molecular dynamics with the use of circular shaped elements. The intergranular normal forces at contacts are calculated through a linear viscoelastic law while the tangential forces are calculated through a perfectly plastic viscoelastic model. A model of rolling friction is incorporated in order to account for the damping of the grains rolling motion. Different boundary conditions of the profile have been implemented; a bedrock at the base, a free surface at the top and periodic boundaries in the horizontal direction. The sand deposit is subjected to a harmonic excitation at the base. Using this model, the fundamental and resonance frequencies of the deposit are first determined. The former is determined from the low-amplitude free vibration and the latter by performing a variable-frequency excitation test. It is noted that there is a significant gap between the two frequencies, this gap could be attributed to the degradation of the soil shear modulus in the vicinity of the resonance. Such degradation is well proven in classical soil dynamics. The effects of deposit height and confinement on resonance frequency and free-surface dynamic amplification factor are then investigated. The obtained results highlighted that the resonance frequency is inversely proportional to the deposit's thickness whereas the dynamic amplification factor R_d increases with the deposit's thickness. In the other hand, when the confinement increases the deposit becomes stiffer, which results in reducing the amplification. Such result is in accordance with theoretical knowledge which states that the most rigid profiles such as rocks do not amplify seismic movement.

Keywords: *micromechanical model, sand deposit, discrete element method, shear wave propagation.*

Received date: 11.04.2024
Accepted date: 27.06.2024
Published date: 29.06.2024

How to cite
Derbane, S., Mansouri, M., Messast, S. (2024). Contribution to micromechanical modeling of the shear wave propagation in a sand deposit. Technology Audit and Production Reserves, 3 (1 (77)), 10–18. doi: https://doi.org/10.15587/2706-5448.2024.301709

1. Introduction

The propagation of seismic waves from bedrock to the free ground surface is strongly influenced by the properties of the soil layers traversed. In particular, the stiffness and damping of these layers have a significant impact on the transmission of motion. For granular soils, these two properties, i. e. stiffness and damping, depend on the characteristics of the applied motion, such as amplitude and frequency, as well as on certain soil state parameters, such as confining and density states. The classical methods used to analyze the transmission of motion and its amplification from bedrock to surface are typically based on continuum mechanics. These methods are effective for cohesive soils, but for granular soils, given their discrete nature, the discrete element models (DEM) can provide more information on the mechanisms involved. DEM is a numerical method that simulates the behavior of granular materials by treating individual particles as discrete entities. This allows to capture the complex interactions between particles, which are essential for understanding the behavior of granular soils. This method has just proved its place in the field of geotechnics through the study of natural phenomena such as the liquefaction of sands under Rayleigh-wave [1–3]. On the other hand, it was used in the field of rail transport to check the stability of the ballasts under cyclical loads [4, 5]. The modeling of wave propagation with DEM has been used to characterize the shear modulus and the damping of granular materials for low frequencies [6]. The parameters influencing the attenuation of wave amplitudes for a set of grains of the same diameter have been also studied using DEM [7]. Simulations of shock-induced load transfer processes in granular media was carried out by in [8]. The wave propagation in granular assemblies with a focus on the effects of particle size and elastic properties on the wave velocity was investigated in [9]. In the same framework, an analysis of the effect of the grain shape on the wave propagation in a granular material was presented in [10] and the influence of force chains on the wave propagation

in cohesion less granular packing was studied [11]. The dynamic force chains were used to recognize the major propagation path of a dynamic load in cohesion less granular materials in [12, 13] and the problem related to the stability of force chains is studied in [14].

The aim of this research is to perform a 2D numerical study the vertical shear wave propagation in a sand deposit. For this purpose, a discrete element model is developed and numerical simulations are conducted to analyze the response of the deposit subjected to harmonic excitation at the base. In order to show certain features of the behavior of granular deposits under harmonic excitations, various parameters are varied, including excitation frequency and amplitude, as well as deposit thickness and confinement.

2. Materials and Methods

The discrete element model employed in this work is based on the molecular dynamics method. It models the granular material at the micromechanical scale using independent elements. The grains of the material interact at the contact points and each grain interacts with its neighbors and develops contact forces. It is assumed that the global deformation of the medium is mainly due to the relative motions of the grains considered as rigid bodies [15, 16]. The choice of a simple shape of the grains plays an important role in the optimization of the modeling time [10]. For the modeling simplicity, the most used shapes are discs for a two-dimensional 2D modeling and spheres for the three-dimensional 3D case. The contact forces are calculated through simple models based on a slight overlap of the grains [17, 18].

2.1. Equations of motion. The movement of the grains is the parameter responsible for the overall behavior of the medium, this movement obeys to the Newton's second law (1), which is used to obtain the accelerations of the grains. These equations are constructed taking into account all external forces, including gravitational and contact forces. The integration of these equations must be carried out gradually with sufficiently short time increments. It is therefore necessary to discretize time in fairly small steps, during which accelerations, velocities and positions are accurately predicted. The evolution of grain displacements from one-time step to another is obtained in two stages; a first prediction step which uses the acceleration at the start of the time step and a second correction step involving the acceleration at the end of the time step. Velocities and positions are corrected according to the change in acceleration during the time step using the «Velocity-Verlet» algorithm.

Grain motions are governed by Newton's second law, which is expressed as follows:

$$\begin{cases} m_i \ddot{\vec{x}}_i = \sum_j \vec{F}_{ij}^{\,contact} + m_i \vec{g}, \\ I_i \ddot{\vec{\varphi}}_i = \sum_j \vec{M}_{ij}^{\,contact}, \end{cases} \quad (1)$$

where $\ddot{\vec{x}}_i$ and $\ddot{\vec{\varphi}}_i$ represent respectively the translational and rotational accelerations of the grains; m_i and I_i are the mass and the moment of inertia respectively; $\vec{F}_{ij}^{\,contact}$ is the interaction force applied by a grain j in contact with grain i; $\vec{g}$ is the acceleration due to gravity; $\vec{M}_{ij}^{\,contact}$ is the moments caused with respect to the center of gravity of grain i by the contact forces $\vec{F}_{ij}^{\,contact}$.

2.2. Law of interaction between grains

2.2.1. Contact forces. A simplified decomposition is used to study contact forces; a normal component $\vec{F}_n$ and a tangential component $\vec{F}_s$ included in the plane tangent to the grain at the point of contact [19]. The evaluation of interaction forces is usually done according to an appropriate interaction laws. The orientation of the tangential force $\vec{F}_s$ is given by the direction of the relative tangential velocity between the two grains at the time of contact.

The Normal Contact Force $\vec{F}_n$ is calculated by a viscoelastic model (Fig. 1):

$$\vec{F}_n = \left(-k_n D_n - \nu_n V_n\right)\vec{n}, \quad (2)$$

where k_n is the elastic stiffness; v_n is the viscous damping constant; V_n is the normal velocity.

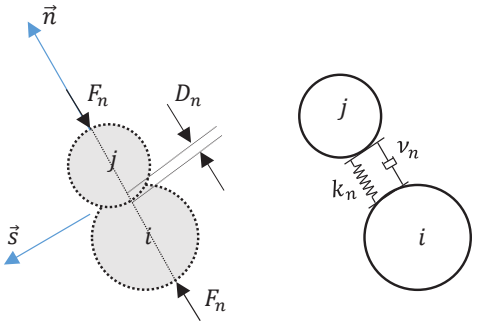

Fig. 1. Normal force modeling between grains

The normal distance between two grains i and j denoted D_n is defined geometrically by:

$$D_n = \vec{x}_j - \vec{x}_i - r_i - r_j, \quad (3)$$

in which r_i and r_j are the radius of grains i and j.

It should be noted that the elastic stiffness and the viscous damping (k_n and ν_n) are chosen in a way to correctly model the behavior of the material. In fact, k_n must be large enough to avoid a substantial overlap which affects the overall behavior, while ν_n controls the damping in the material, it is calculated from the coefficient of restitution ε_n which represents the ratio between the separation velocity (rebound velocity) V_{ns} and the contact initiation velocity (impact velocity) V_{n0}. The value of this coefficient is naturally between 0 and 1. Thus, the viscous damping coefficient ν_n is obtained as a function of the restitution coefficient according to equation [16]:

$$\nu_n = -\frac{2\log(\varepsilon_n)\sqrt{k_n m_{eff}}}{\sqrt{\pi^2 + (\ln \varepsilon_n)^2}}, \quad (4)$$

in which m_{eff} is effective mass calculated as:

$$m_{eff} = \frac{m_i m_j}{(m_i + m_j)}, \quad (5)$$

where m_i and m_j are the masses of the two contacting grains.

The tangential contact force is calculated by a viscoelastic model with slip (Fig. 2) [20], $\vec{F}_s$ is given by:

$$\vec{F}_s = \min(k_s D_s + v_s V_s, \mu_d F_n)\vec{s}, \quad (6)$$

 ISSN 2664-9969

where k_s is the tangential stiffness; v_s the viscous damping coefficient; μ_d is the inter-particle coefficient of friction; D_s is the grain deformation due to shear force; V_s is the tangential velocity of grain j with respect to grain i.

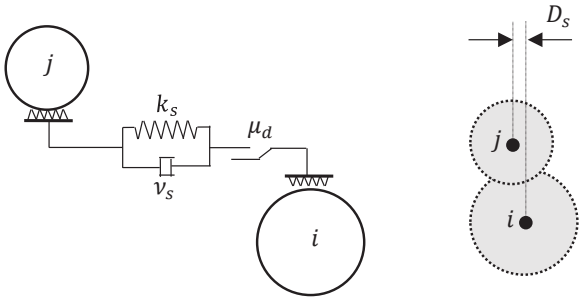

Fig. 2. Shear force between grains

2.2.2. Contact duration. The duration of a contact t_c is half the natural period of the oscillator and can be expressed as:

$$t_c = \pi\sqrt{\frac{m_{eff}}{k_n}}. \quad (7)$$

This contact duration t_c is of practical importance. Indeed, the integration of the equations of motion is only stable if the integration time step Δt is sufficiently small compared to t_c, in other words the evolution of the contact should be well described. Otherwise, calculation instabilities may occur due to late detection or even non-detection of contacts. To avoid these instabilities, it is common to discretize the duration of the contact t_c at least in ten-time steps [16]:

$$\Delta t_{max} \approx 0.1\pi\sqrt{\frac{m}{k_n}}, \quad (8)$$

where m is the smallest effective mass in the system.

2.3. Wave propagation modeling. The model used for the modeling of vertical shear wave propagation in a sand deposit implemented on a C^{++} code.

First, the sand grains are pluviated under gravity to form a dense deposit, with using different boundary conditions. Periodic boundaries have been introduced to represent an infinite profile in the horizontal direction, the upper surface is considered free and the profile is limited and supported at the base by a wall which is considered as bedrock. A chain of grains is introduced onto this bedrock, through which a controlled horizontal displacement is applied. The interactions between the grains of the chain and the deposit grains are treated with the same interaction models used in the interactions of the deposit grains.

In order to study the shear wave propagation in the profile, a harmonic displacement with controlled amplitude and frequency is applied to the grain chain at the bottom of the deposit. Finally, the deposit is divided into a defined number of layers in which the average displacements is monitored during the excitation of the profile.

3. Results and Discussion

3.1. Model Parameters. Fig. 3 shows the sand deposit model to be subjected to a base excitation, the different boundary conditions are indicated.

The properties of the grains as well as the micromechanical parameters used in the computation of the contact forces between the grains are presented in Table 1.

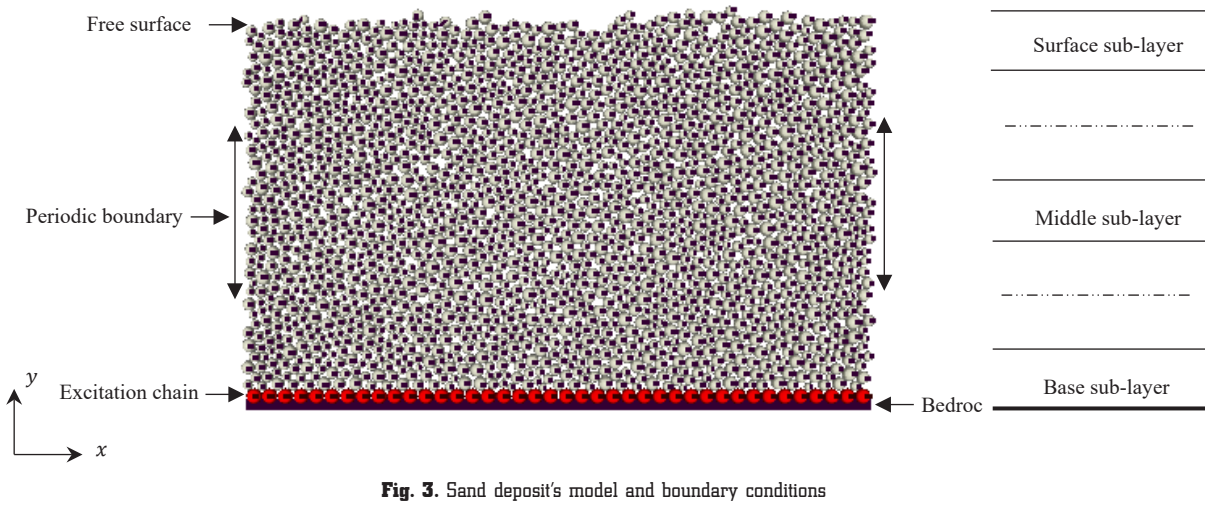

Fig. 3. Sand deposit's model and boundary conditions

Table 1

Simulation parameters

Parameters	Value
Grains number	5000
Grain radius r_i	$1.00{\cdot}10^{-3}$ to $2.00{\cdot}10^{-3}$ m
Density G_s	2600 kg/m^3
Contact normal stiffness k_n	$1.2{\cdot}10^6$ N/m
Contact shear stiffness k_s	$9.6{\cdot}10^5$ N/m
Inter-particle friction coefficient μ	0.5

The width of the deposit (period) is set to 2.0 m. With the used number of 5000 grains, the obtained deposit's high is about 0.53 m.

Once the deposit is built, it is subjected to a harmonic excitation at its base $u(t)=A_0\sin(ft)$ with $A_0=4\cdot10^{-4}$ m and $\omega=20$ rad/s. The dynamic amplification factor (R_d) at the top layer of the deposit is defined as:

$$R_d=\frac{A}{A_0}, \tag{9}$$

where A denotes the displacement amplitude at the free surface; A_0 is the displacement amplitude at the bedrock, i. e. the base excitation.

3.2. Analysis of vibrational properties of the sand deposit's model. In order to avoid the perturbations due to transient response of the profile, the amplitude of the excitation is gradually increased during 4.5 seconds to reach a maximum of $4\cdot10^{-4}$ m, maintained for 6 seconds before gradually decreasing and reaching zero during 1.5 seconds (Fig. 4, *a*). The monitoring of the horizontal motion propagation throughout the deposit is carried out by dividing the profile into 10 sub-layers. The average displacement in each sub-layer is monitored during and after the excitation.

Fig. 4, *b* presents the displacement at top sub-layer during the excitation. By comparing the amplitude of the displacement at this layer with that of the excitation, it is clear that the introduced excitation movement is amplified at the free surface. Fig. 4, *b* shows also that the soil experiences a damped vibration after ending the excitation, this means that the deposit exhibits an elastic damped behavior.

The fundamental frequency of a deposit is usually estimated using low vibration amplitudes. For the present modeling, the fundamental frequency of the deposit can be estimated from the free vibration phase resulting after stopping the excitation. Fig. 5 shows a zoom of the displacement history in this phase.

The period of vibration estimated from the displacement plot is approximately $T=0.1642$ s. This period corresponds to a natural frequency $\omega=2\pi/T=38.265$ rad/s. From this frequency, it is possible to estimate the shear wave velocity in the deposit [21] using the formula $c=4H/T=12.833$ m/s.

On the other hand, it is possible to estimate deposit's ratio for small vibration amplitudes using the logarithmic decrement expressed as [22]:

$$\xi=\frac{1}{\sqrt{1+\left(\frac{2\pi}{\delta}\right)^2}}. \tag{10}$$

With

$$\delta=\ln\left(\frac{Y_{\max(i)}}{Y_{\max(i+1)}}\right), \tag{11}$$

in which δ is the logarithmic decrement; $Y_{\max(i)}$ and $Y_{\max(i+1)}$ are two successive pics in the free vibration.

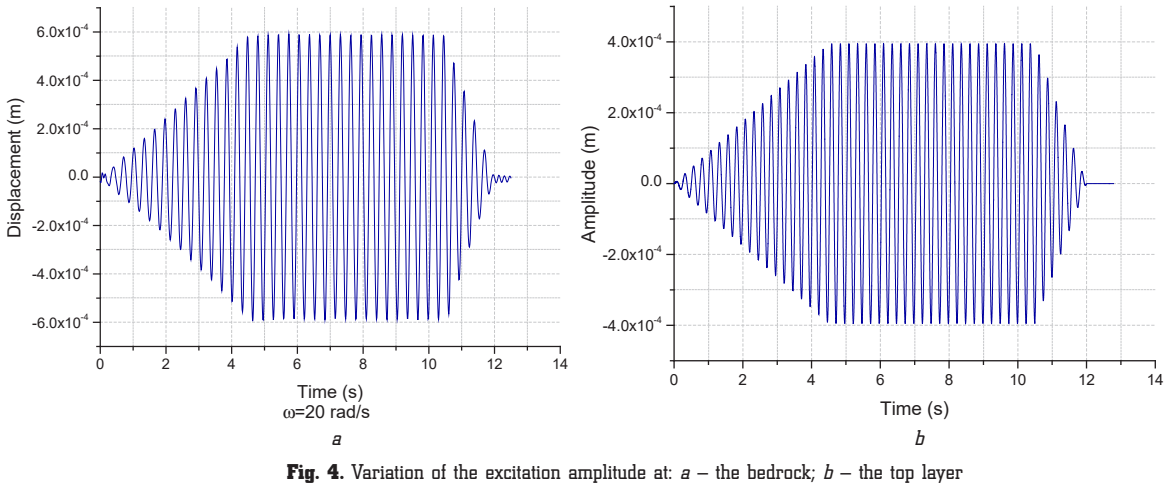

Fig. 4. Variation of the excitation amplitude at: *a* – the bedrock; *b* – the top layer

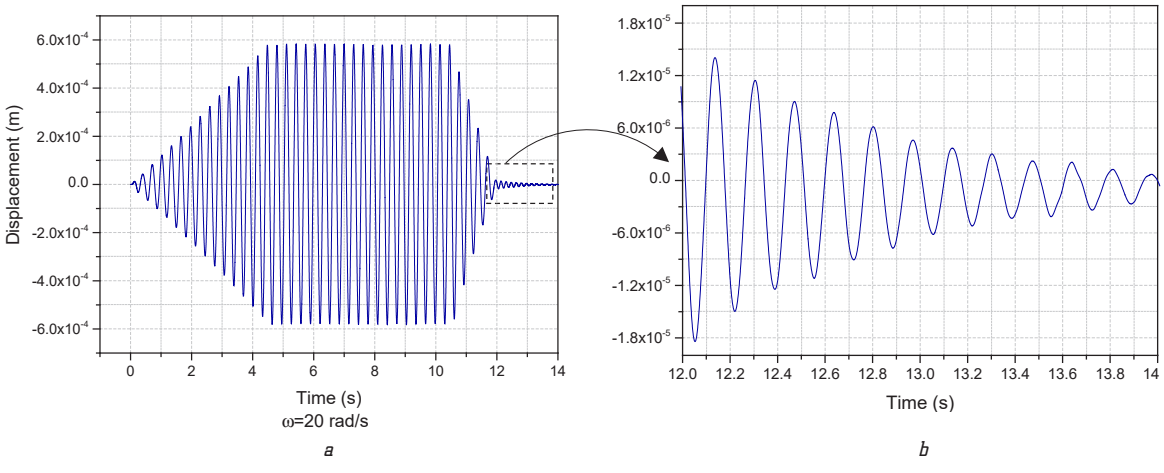

Fig. 5. Top layer time history response: *a* – total response; *b* – zoom of free vibration part

ISSN 2664-9969

The calculations based on the response curve of Fig. 5, give the damping ratio:

$$\xi = \frac{1}{\sqrt{1+\left(\frac{2\pi}{0.2292}\right)^2}} = 3.65\ \%.$$

This low amplitude of free vibrations could be considered as damped elastic vibrations. Based on the low obtained damping value, one would expect the resonant frequency to be slightly lower but not far from the fundamental frequency which is around 38.265 rad/s.

Fig. 6 shows a part of the steady state response $(6\ \text{s} \le t \le 7\ \text{s})$ at the base, the middle and the top layers.

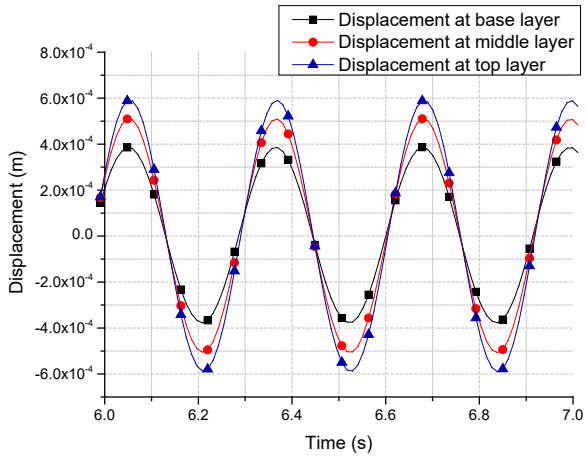

Fig. 6. Variation of displacement from the base to the surface

It is possible to note in Fig. 6 the presence of progressive amplification of the motion from the base to the surface. The amplification ratio (R_d) of the maximum displacement is at the top sub-layer with a value of 1.47.

Fig. 7 shows the evolution of the dynamic amplification factor versus the height with respect to the bedrock.

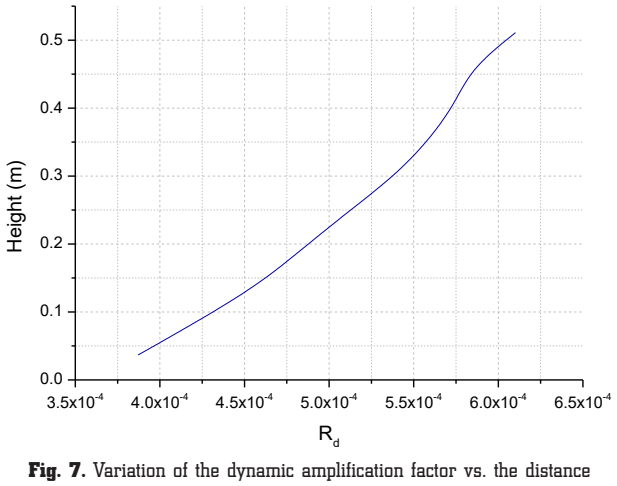

Fig. 7. Variation of the dynamic amplification factor vs. the distance from the bedrock

Fig. 7 clearly highlights the movement amplification from the bedrock up to the free surface. Furthermore, it reveals that the used excitation frequency is lower than the first natural frequency (fundamental frequency) of the deposit.

3.3. Influence of the excitation frequency. To investigate the influence of excitation frequency on the deposit response and estimate the first resonance frequency, various excitations with frequencies ranging from 10 rad/s to 35 rad/s were applied. Fig. 8 shows the evolution of the dynamic amplification factor at the top layer in the steady-state phase.

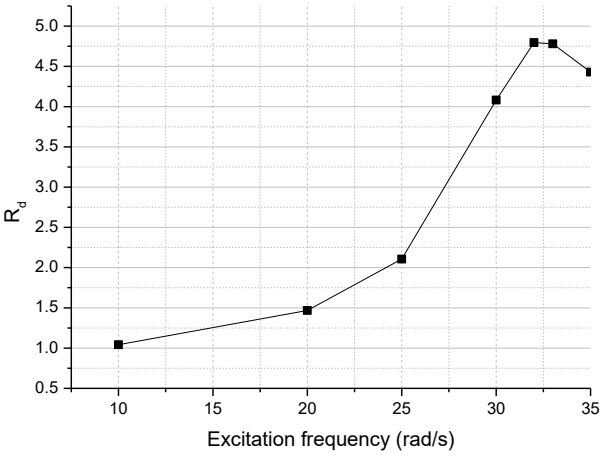

Fig. 8. Dynamic amplification factor at the top layer vs. excitation frequency

Fig. 8 shows that with the increase of the excitation frequency, R_d increases, it reaches a peak, and then it decreases. The first resonance frequency corresponds to the maximum value of the amplification; it is approximately equal to 33 rad/s. It may be noted that this is quite low compared to the fundamental frequency estimated above from the low-amplitude free vibration. This difference is probably due to the degradation of the shear modulus at high vibration amplitudes.

3.4. Influence of the thickness of the deposit

3.4.1. Influence on the movement amplification. In the aim to study the influence of the deposit thickness on the movement amplification at the surface, five thicknesses were studied (0.53 m, 0.70 m, 0.85 m, 1.02 m and 1.97 m). These thicknesses are obtained by varying the width of the deposit while keeping the same number of grains. The deposit is subjected to a harmonic excitation with amplitude $A_0 = 4 \cdot 10^{-4}\text{m}$ and excitation frequency $\omega = 25\,\text{rad/s}$.

Fig. 9 presents the variation of the dynamic amplification factor (R_d) with deposit thicknesses.

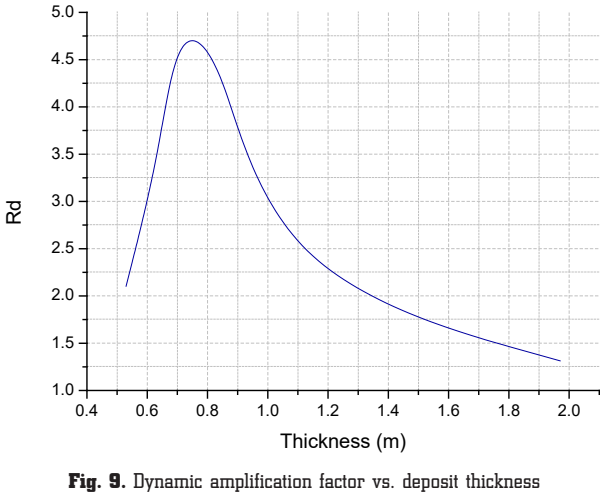

Fig. 9. Dynamic amplification factor vs. deposit thickness

Fig. 9 shows that with increasing thickness, R_d increases initially, it reaches a maximum then it decreases. This plot highlights the change in fundamental frequency with thickness. At thicknesses where the fundamental frequency is close to the excitation frequency, resonance occurs, corresponding to the peak on the graph. For this application, it can be understood that for a deposit's thickness about 0.75 m, the resonance frequency is 25 rad/s.

3.4.2. Influence on the resonance frequency. In order to study the influence of the deposit thickness on the resonance frequency, four thicknesses were studied (0.53 m, 0.64 m, 0.74 m and 1.00 m). These thicknesses are obtained by varying the width of the deposit while keeping the same number of grains. The deposit is subjected to a harmonic excitation with amplitude $A_0 = 2 \cdot 10^{-4}$ m and different excitation frequency ω (8 rad/s to 25 rad/s).

Fig. 10 presents the variation of the dynamic amplification factor (R_d) with deposit thicknesses and excitation frequency.

Fig. 10 shows that with increasing thickness, R_d initially increases, reaches a maximum, then decreases. It clearly highlights the change in resonance frequency with thickness. For each thickness, when the excitation frequency is close to the fundamental frequency, resonance occurs, corresponding to peaks on the graphs.

These graphs indicate therefore, that the resonance frequency is inversely proportional to the thickness and that the dynamic amplification factor R_d increases with the deposit's thickness.

3.5. Influence of the deposit's confinement on the wave propagation. Deep soil layers are naturally subjected to confining pressures. To simulate this case, a weighing chain of grains is introduced at the surface of the deposit; the confining stress could be increased through the increase of the specific weight of the chain grains. In this application, the deposit is subjected to a harmonic excitation with amplitude $A_0 = 4 \cdot 10^{-4}$ m, excitation frequency $\omega = 30$ rad/s and confining pressures ranging from 10000 kPa to 80000 kPa.

Fig. 11 shows a part of the steady state response $(7\ \text{s} \le t \le 8\ \text{s})$ of displacement time history of the top layer for different confining pressures.

Fig. 11 highlights the decrease of the displacement amplification at the top layer with the increase in confining pressure. Fig. 12 shows the variation of the dynamic amplification ratio following the confining pressure change.

Fig. 12 shows clearly that the dynamic amplification factor R_d decreases with the increase of the confinement.

This indicates that the deposit becomes stiffer when the confinement increases, which results in reducing the amplification. This result is in accordance with theoretical knowledge which states that the most rigid profiles such as rocks do not amplify seismic movement.

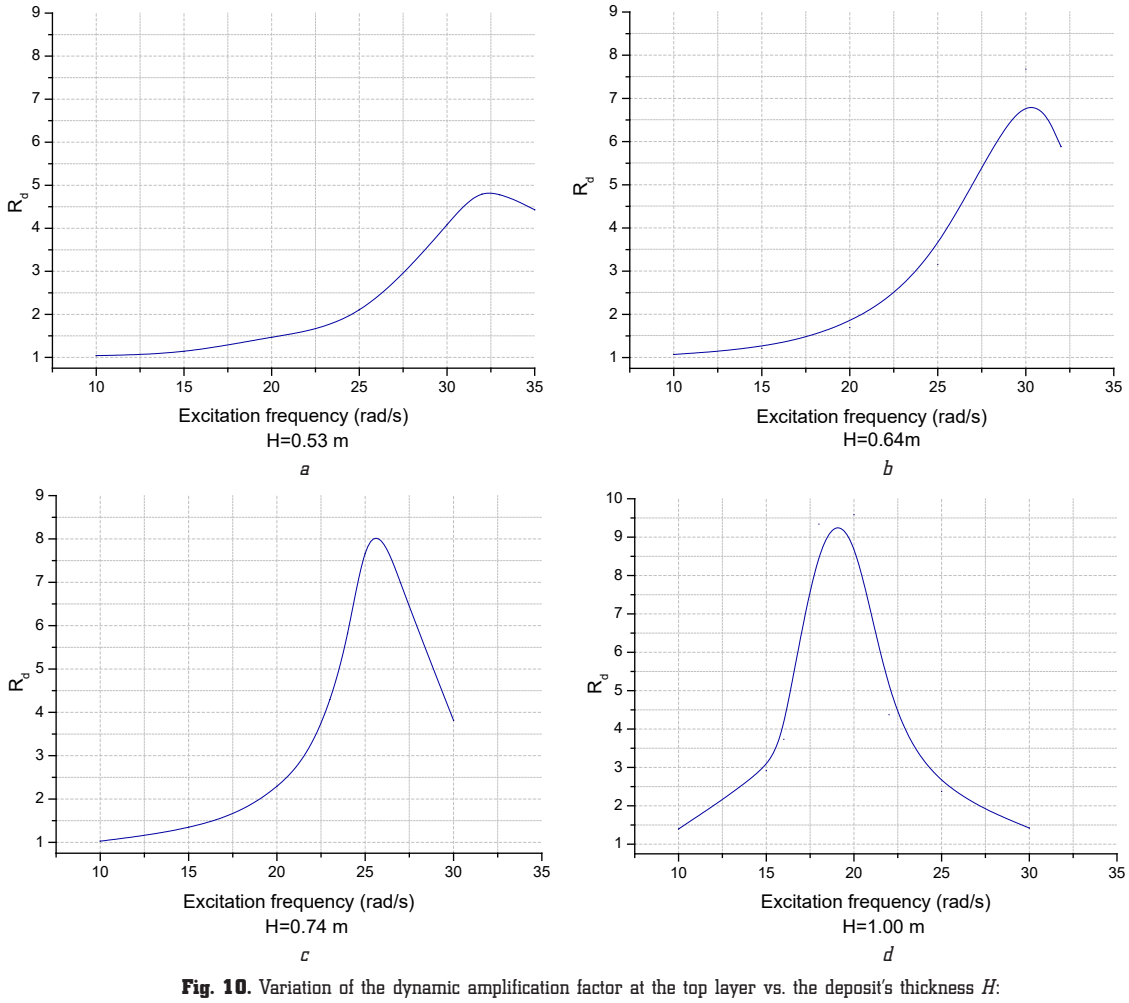

Fig. 10. Variation of the dynamic amplification factor at the top layer vs. the deposit's thickness H: *a* – H=0.53 m; *b* – H=0.64 m; *c* – H=0.74 m; *d* – H=1.00 m

ISSN 2664-9969

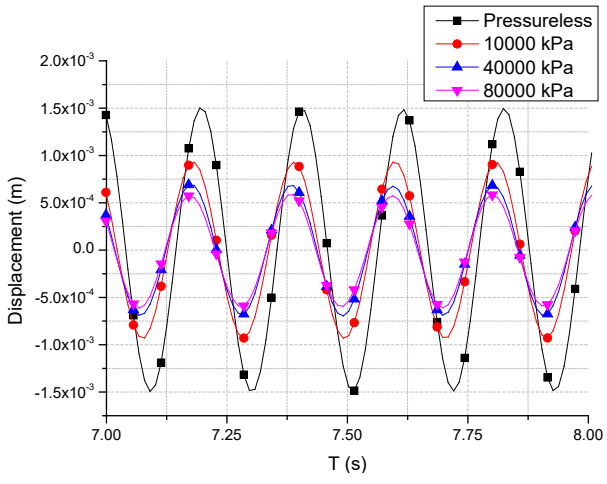

Fig. 11. Effect of surface confinement pressure on the evolution of displacement

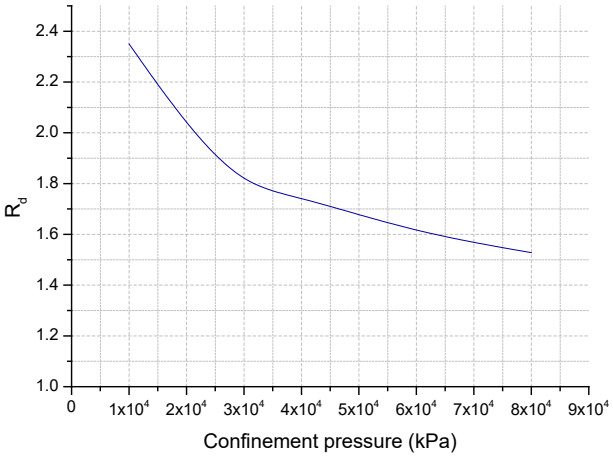

Fig. 12. Variation of the dynamic amplification factor (R_d) at top layer vs. confining pressure

In order to study the change in confinement effect with excitation frequency, two frequencies (20 rad/s and 30 rad/s) were used for a deposit with confining pressures of 0 and 10 000 kPa. Fig. 13 shows parts of the steady-state response of the displacement time history at the top layer for the two excitation frequencies.

Fig. 13 shows that the effect of confinement on amplification is sensitive to the excitation frequency. For the studied case, it could be understood that the frequency of 20 rad/s is sufficiently low compared to the resonance frequency of the pressureless deposit, so amplification is low. Increased confinement stiffens the deposit and makes the resonance frequency further away from the excitation frequency, resulting in a small reduction in amplification. On the other hand, the frequency of 30 rad/s is close to the resonance frequency of the deposit, so amplification is initially high. In this case, confinement moves the resonance frequency away from the excitation frequency, significantly reducing amplification. Finally, this section concludes by showing that deposit behavior is highly dependent on confinement. Thus, the behavior of a granular soil layer is strongly affected by its depth in the soil profile.

3.6. Variation of the amplification at the free surface with the excitation frequency and amplitude. Several simulations have been performed by using the initial deposit and changing the excitation amplitude and the frequency. The amplitude is varied from $8{\cdot}10^{-5}$ m to $1{\cdot}10^{-3}$ m for frequencies of 15 rad/s, 20 rad/s, 25 rad/s, and 30 rad/s. Unlike elastic deposits, the simulation showed that the amplification is affected by the excitation amplitude.

To see how the dynamic amplification factor varies with the two excitation parameters, a fitting function is developed following the model:

$$R_d = \left(a \cdot A^b\right)\left(\omega^c \cdot d^{\omega}\right), \tag{12}$$

where R_d is dynamic amplification factor; A is excitation amplitude; ω is excitation frequency.

Using the results of all the simulations, the model coefficients obtained are given in Table 2.

Table 2

Model parameters

Coefficient	Value
a	1180.160
b	0.149435
c	–3.45735
d	1.27231

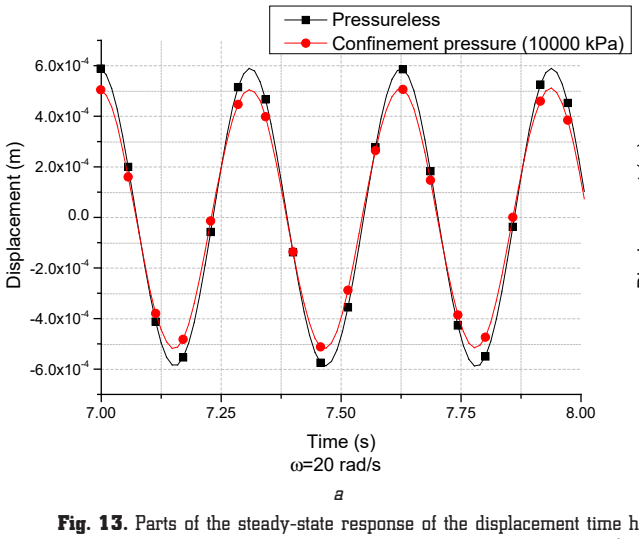

a

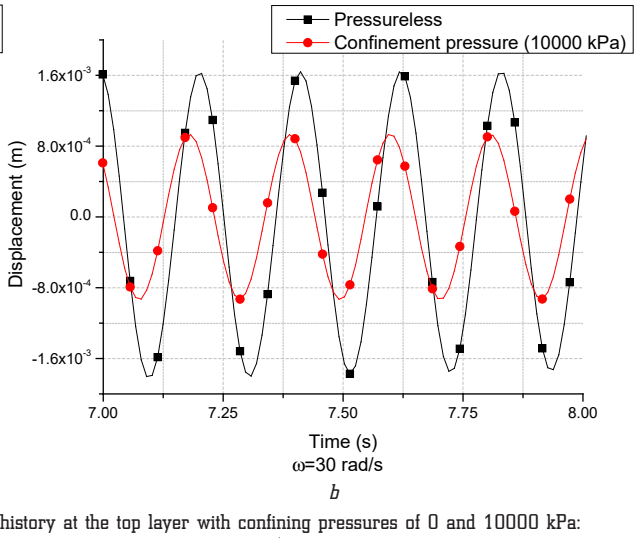

b

Fig. 13. Parts of the steady-state response of the displacement time history at the top layer with confining pressures of 0 and 10000 kPa: *a* – excitation frequency 20 rad/s; *b* – excitation frequency 30 rad/s

Fig. 14 presents the correlation between the values of the dynamic amplification factor R_d obtained from the DEM simulation and R_d from the fitting function (12).

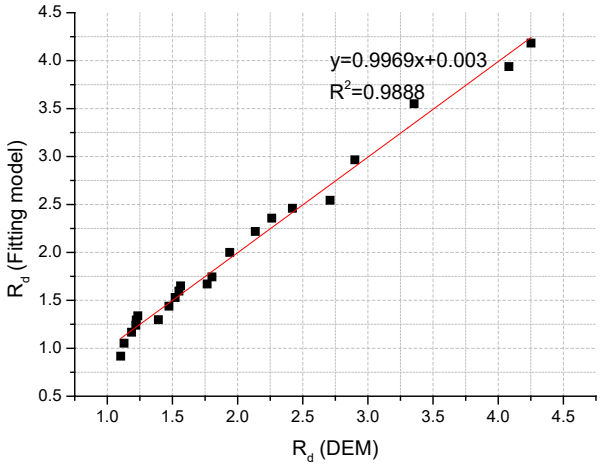

Fig. 14. R_d fitting model from DEM simulations

Fig. 14 shows a linear correlation with a and a correlation coefficient of $R^2 = 0.9888$. Therefore, the obtained fitting function enables the dynamic amplification factor to be correctly estimated as a function of excitation amplitude and frequency. It should be noted that this work is done only for excitation frequencies below the fundamental frequency.

3.7. Discussion. In this research work, we have presented a model based on the discrete element method for simulating wave propagation in a granular soil deposit. The advantage of this type of model is that it inherently considers the discontinuous aspect of the material and, consequently, the intergranular slippage that occurs during large deformations, as in the case of vibrations in the vicinity of resonance. The performed simulations using this model reflect well-established vibratory properties on the subject of wave propagation in soil deposits such as:

– The movement amplification that increases from the bedrock up to the free ground surface for low frequencies, as shown in Fig. 7.

– The phenomenon of resonance and the frequency of resonance, by performing a variable-frequency vibration test that gives the typical response presented in Fig. 8.

– The thickness dependence of the dynamic amplification factor and resonance frequency, as thicker deposits are more flexible (Fig. 9 and Fig. 10).

– The decrease of the dynamic amplification factor with increasing confinement pressure, which makes the deposit stiffer (Fig. 12).

Furthermore, given the fundamental frequency and damping factor obtained from the free vibration response in section 3.2 (ω=38.265 rad/s and ξ=3.85 %), the resonance frequency should be very close to the fundamental frequency, as reported in reference [21]. However, it was found that the resonance frequency obtained from the variable-frequency vibration test in section 3.3 (ω≈33 rad/s) is significantly lower than the fundamental frequency of the deposit. This is due possibly to the degradation of the soil shear modulus in the vicinity of the resonance. This finding underlines the need to consider the effect of shear modulus degradation in a rational way when calculating the response of soil deposits. It should be noted that this issue is commonly studied in earthquake engineering through continuum mechanics using approximate behavior models.

Finally, as with any numerical modeling, the model used in this work involves simplifications. It is possible to believe that the most important simplifications here are firstly the 2D nature of the model and secondly the circular shape of the grains. Although the results obtained are interesting, it would be worthwhile to carry out similar investigations using a 3D model and element shapes closer to those of real grains. Through this modeling approach, it would also be interesting to characterize the degradation of shear modulus as a function of strain level for soils with different micromechanical properties such as grain shape, contact friction and intergranular cohesion. Such degradation characterization could even be a valuable addition to the continuum-based models commonly used in this field.

4. Conclusions

The Discrete Element Model presented in this paper deals with a two-dimensional modeling of wave propagation in a granular material deposit. Several simulations have been performed to understand the response of granular materials to applied harmonic excitations at the bedrock. Different parameters affecting the dynamic response of the deposit are analyzed namely, the excitation frequency, the thickness and the confinement of the deposit.

The performed simulations highlighted several response aspects such as the amplification of the exciting movement from the bedrock up to the free surface, the resonance situation when the excitation frequency becomes close to the fundamental frequency and the change of the fundamental frequency with deposit's thickness and confinement. The simulation showed that for a granular deposit, the resonance frequency is quite low compared to the fundamental frequency, this is probably due to the degradation of the shear modulus of the material with the strain increase near the resonance. With regard to confinement, it is shown that the behavior of a granular soil layer is strongly affected by the confining pressure applied on it, i. e. by its depth in the soil profile.

For the used granular deposit, it is shown that it is possible to obtain a linear fitting equation that correlate the dynamic amplification factor to the amplitude and frequency of the excitation below the first natural frequency. Such a function can serve as an easy tool for estimating amplification instead of going through simulations.

Conflict of interest

The authors declare that they have no conflict of interest in relation to this research, whether financial, personal, authorship or otherwise, that could affect the research and its results presented in this paper.

Financing

The research was performed without financial support.

Data availability

The manuscript has no associated data.

Use of artificial intelligence

The authors confirm that they did not use artificial intelligence technologies when creating the current work.

References

1. Jiang, M., Kamura, A., Kazama, M. (2022). Numerical study on liquefaction characteristics of granular materials under Rayleigh-wave strain conditions using 3D DEM. *Soils and Foundations, 62 (4),* 101176. doi: https://doi.org/10.1016/j.sandf.2022.101176
2. Cui, J., Men, F., Wan, X. (2004). Soil liquefaction induced by Rayleigh wave. *13th World Conference on Earthquake Engineering.*
3. Nakase, H., Takeda, T., Oda, M. (1999). A simulation study on liquefaction using DEM. *Proceedings of the 2nd International Conference on Earthquake Geotechnical Engineering,* 637–642.
4. Guo, Y., Zhao, C., Markine, V., Jing, G., Zhai, W. (2020). Calibration for discrete element modelling of railway ballast: A review. *Transportation Geotechnics, 23.* doi: https://doi.org/10.1016/j.trgeo.2020.100341
5. Kumar, N., Suhr, B., Marschnig, S., Dietmaier, P., Marte, C., Six, K. (2019). Micromechanical investigation of railway ballast behavior under cyclic loading in a box test using DEM: Effects of elastic layers and ballast types. *Granular Matter, 21,* 106. doi: https://doi.org/10.1007/s10035-019-0956-9
6. Zamani, N., El Shamy, U. (2011). Analysis of wave propagation in dry granular soils using DEM simulations. *Acta Geotechnica, 6 (3),* 167–182. doi: https://doi.org/10.1007/s11440-011-0142-7
7. Sadd, M. H., Adhikari, G., Cardoso, F. (2000). DEM simulation of wave propagation in granular materials. *Powder Technology, 109 Ž2000,* 222–233. doi: https://doi.org/10.1016/s0032-5910(99)00238-7
8. Sakamura, Y., Komaki, H. (2011). Numerical simulations of shock-induced load transfer processes in granular media using the discrete element method. *Shock Waves, 22 (1),* 57–68. doi: https://doi.org/10.1007/s00193-011-0347-6
9. Ning, Z., Khoubani, A., Evans, T. M. (2015). Shear wave propagation in granular assemblies. *Computers and Geotechnics, 69,* 615–626. doi: https://doi.org/10.1016/j.compgeo.2015.07.004
10. Tang, X., Yang, J. (2021). Wave propagation in granular material: What is the role of particle shape? *Journal of the Mechanics and Physics of Solids, 157,* 104605. doi: https://doi.org/10.1016/j.jmps.2021.104605
11. Peters, J. F., Muthuswamy, M., Wibowo, J., Tordesillas, A. (2005). Characterization of force chains in granular material. *Physical Review E, 72 (4).* doi: https://doi.org/10.1103/physreve.72.041307
12. Fu, L., Zhou, S., Guo, P., Wang, S., Luo, Z. (2019). Induced force chain anisotropy of cohesionless granular materials during biaxial compression. *Granular Matter, 21 (3).* doi: https://doi.org/10.1007/s10035-019-0899-1
13. Fu, L., Zhou, S., Zheng, Y., Zhuang, L. (2023). Characterizing dynamic load propagation in cohesionless granular packing using force chain. *Particuology, 81,* 135–148. doi: https://doi.org/10.1016/j.partic.2023.01.007
14. Campbell, C. S. (2003). A problem related to the stability of force chains. *Granular Matter, 5 (3),* 129–134. doi: https://doi.org/10.1007/s10035-003-0138-6
15. Pöschel, T., Schwager, T. (2005). *Computational Granular Dynamics – Models and Algorithms.* Berlin, Heidelberg: Springer-Vrlag.
16. Mansouri, M., El Youssoufi, M. S., Nicot, F. (2016). Numerical simulation of the quicksand phenomenon by a 3D coupled Discrete Element – Lattice Boltzmann hydromechanical model. *International Journal for Numerical and Analytical Methods in Geomechanics, 41 (3),* 338–358. doi: https://doi.org/10.1002/nag.2556
17. Richefeu, V. (2005). *Approche par éléments discrets 3D du comportement de matériaux granulaires cohésifs faiblement contraints.* Thèse Université Montpellier II – Sciences et Techniques du Languedoc.
18. Cundall, P. A., Strack, O. D. L. (1979) A discrete numerical model for granular assemblies. *Géotechnique, 29 (1),* 47–65. doi: https://doi.org/10.1680/geot.1979.29.1.47
19. Delenne, J., El Youssoufi, M. S., Cherblanc, F., Bénet, J. (2004). Mechanical behaviour and failure of cohesive granular materials. *International Journal for Numerical and Analytical Methods in Geomechanics, 28 (15),* 1577–1594. doi: https://doi.org/10.1002/nag.401
20. Semblat, J. F., Luong, M. P. (1998). Wave propagation through soils in centrifuge testing. *Journal of Earthquake Engineering, 2 (10),* 147–171. doi: https://doi.org/10.1080/13632469809350317
21. Verruijt, A. (2009). *An introduction to soil dynamics (Vol. 24).* Springer Science & Business Media. doi: https://doi.org/10.1007/978-90-481-3441-0
22. Acton, J. R., Squire, P. T. (1985) *Solving Equations with Physical Understanding.* Bristol: Adam Hilger Ltd., 219.

✉***Said Derbane,*** *Postgraduate Student, Department of Civil Engineering, LMGHU Laboratory, University of 20 August 1955 Skikda, Skikda, Algeria, e-mail: derbane_said@yahoo.fr, ORCID: https://orcid.org/0009-0003-7773-5806*

Mouloud Mansouri, *Associate Professor, Civil Engineering Research Laboratory of Setif (LRGCS), Department of Civil Engineering, Ferhat Abbas University of Setif, Setif, Algeria, ORCID: https://orcid.org/0000-0002-4179-7488*

Salah Messast, *Professor, Department of Civil Engineering, LMGHU Laboratory, University of 20 August 1955 Skikda, Skikda, Algeria, ORCID: https://orcid.org/0000-0002-0864-2257*

✉*Corresponding author*